Diamond & Related Materials 44 (2014) 123–128

Contents lists available at ScienceDirect

Diamond & Related Materials

journal homepage: www.elsevier.com/locate/diamond

Interface and interlayer barrier effects on photo-induced electron emission from low work function diamond films

Tianyin Sun [a], Franz A.M. Koeck [a], Petr B. Stepanov [a,b,c], Robert J. Nemanich [a,*]

[a] Department of Physics, Arizona State University, Tempe, AZ 85287-1504, USA
[b] Technological Institute for Superhard and Novel Carbon Materials, Troitsk, Moscow Region 142190, Russia
[c] Moscow Institute of Physics and Technology, Dolgoprudny, Moscow Region 141700, Russia

ARTICLE INFO

Article history:
Received 18 November 2013
Received in revised form 3 February 2014
Accepted 11 February 2014
Available online 26 February 2014

Keywords:
Doped diamond
Photo-induced emission
Thermionic emission
PEEM

ABSTRACT

Nitrogen-doped diamond has been under investigation for its low effective work function, which is due to the negative electron affinity (NEA) produced after surface hydrogen termination. Diamond films grown by chemical vapor deposition (CVD) have been reported to exhibit visible light induced electron emission and low temperature thermionic emission. The physical mechanism and material-related properties that enable this combination of electron emission are the focus of this research. In this work the electron emission spectra of nitrogen-doped, hydrogen-terminated diamond films are measured, at elevated temperatures, with wavelength selected illumination from 340 nm to 450 nm. Through analysis of the spectroscopy results, we argue that for nitrogen-doped diamond films on metallic substrates, photo-induced electron generation at visible wavelengths involves both the ultra-nanocrystalline diamond and the interface between the diamond film and metal substrate. Moreover, the results suggest that the quality of the metal–diamond interface can substantially impact the threshold of the sub-bandgap photo-induced emission.

1. Introduction

Diamond is unusual for its property of obtaining a negative electron affinity (NEA) surface after hydrogen passivation [1–3]. With an NEA and *n*-type doping, a low effective work function can be achieved, which enables thermionic electron emission from the diamond surface at relatively low temperatures (<500 °C). Current state-of-the-art techniques for preparing nitrogen-doped diamond thermionic electron emitters involve introducing sufficient sp^2 bonds at the grain boundaries to reduce the upward band bending, and an effective work function of 1.3 eV has been reported [4]. Low energy photons have also produced electron emission from N-doped diamond films. This visible light photo-induced emission from N-doped diamond was found to share the same low threshold energy as the thermionic emission [5]. Combining these emission mechanisms may enable applications in thermionic energy conversion [6,7], and use as a photocathode [8].

A recent study suggested that photon-enhanced thermionic emission (PETE) [9] could be an advantage for combining photo-induced and thermionic emission processes in a novel device structure. Application in a concentrated solar cell was suggested. The proposed cell is composed of two parallel plates serving as the electron emitter and collector, and a vacuum gap that separates the two plates. Solar light illuminates the emitter to induce PETE. According to Ref. [9], in this structure the electron affinity of the semiconductor emitter provides a significant contribution to its PETE efficiency. Based on this effect we proposed that, by coating a semiconductor with a low work function diamond film, high efficiency solar energy conversion could be achieved due to the reduced emission threshold [5]. Efficient transport of electrons through the interface between the substrate and the diamond film thus becomes a key objective in engineering the related materials. Understanding the effect of film structure on the photo-induced emission from the diamond emitters will be crucial in the further development of such multilayer structures. In this work we report a spectroscopic study of photo-induced and thermionic electron emission from N-doped diamond films on metal substrates with different interface and interlayer conditions.

2. Experiment

In this research, microwave plasma enhanced chemical vapor deposition (MPCVD) was employed to prepare nitrogen-doped diamond emitters on 25 mm diameter molybdenum substrates. Four variations were prepared for comparison of different interface structures. They include: 1) a combination of mirror polished Mo substrate/nitrogen-incorporated ultra nanocrystalline diamond ((N)UNCD) inter-layer/N-doped polycrystalline diamond (N-diamond) surface layer; 2) bead-blasted Mo substrate/(N)UNCD/N-diamond; 3) bead-blasted Mo substrate/(N)UNCD; and 4) polished Mo substrate/nanodiamond/N-diamond. The four

* Corresponding author at.
E-mail address: robert.nemanich@asu.edu (R.J. Nemanich).

http://dx.doi.org/10.1016/j.diamond.2014.02.008
0925-9635/

variations are designated by "D1", "D2", "D3" and "D4". Details of the deposition process are described elsewhere [4]. Films of the same structure as D1 were used previously in photo-induced emission studies of N-doped diamond electron emitters [5,10]. Bead-blasted Mo substrates have a significantly higher surface roughness, and have been typically employed in prior thermionic emission measurements of N-doped diamond [11]. The nanodiamond layer was deposited under the same parameters as the (N)UNCD, except argon gas was not introduced during the growth process. The (N)UNCD layer has a typical grain size of 2–5 nm, while the nanodiamond layer has a nanocrystalline structure with a grain size between 10 and 50 nm [12]. The top N-doped diamond layer was deposited under growth conditions for polycrystalline diamond with predominantly sp^3 bonding. Therefore, comparison between D1 and D2 represents a similar diamond film structure on differently treated Mo substrates, while D1 and D4 share the same Mo substrate properties but with different diamond interlayers. After growth, the samples were exposed to a hydrogen plasma. This process provides hydrogen termination that leads to an NEA surface, and consequently a low effective work function of the film.

To study the optical absorption in the diamond layers, a set of samples were prepared for UV–vis spectroscopy measurements. This included a sample with (N)UNCD + N-diamond layers and a sample with only the (N)UNCD layer. Both were grown on polished fused silica substrates, following the same growth conditions as sample D1. Due to the transparency of the substrates, it was difficult to measure the layer thickness using *in situ* laser reflection interferometry (LRI). The thickness of the (N)UNCD layer was empirically estimated to be ~500 nm, and that of the N-doped diamond layer was between 300 and 400 nm. The absorbance data was obtained using a Perkin-Elmer Lambda 18 UV–vis spectrometer.

For spectroscopic electron emission measurements, the diamond samples were transferred into a UHV chamber for measurements of the photo-induced and thermionic electron emission characteristics. A toroidal tungsten coil beneath the sample holder was used for heating the sample, and the sample temperature was measured with a thermocouple positioned at the center behind the substrate holder. The thermocouple temperature was calibrated with a Mikron M90Q infrared pyrometer. Two photon sources were employed in the experiments. A He discharge lamp was optimized for generation of He I (21.2 eV) photons, which were delivered to the sample surface through a ~1.5 mm diameter quartz capillary. An Oriel 100 W ozone-free Xe arc lamp, fitted with band pass filters ranging from 340 to 450 nm, provided photon illumination at an angle of ~35° to the normal direction. The filters had an FWHM of ~10 nm. A VSW-HA50 hemispherical electron analyzer positioned normal to the surface was employed to acquire the photo-induced and thermionic emission spectra. The analyzer was operated at resolutions of ~0.15 or 0.25 eV to achieve appropriate signal intensity. A negative 15 V bias was applied to the sample surface to maximize the collection of the low energy electrons. Prior to spectroscopic emission measurements, the samples were heated to 450 °C for 15 min and then cooled in vacuum. Previous results indicate that water and hydrocarbon contamination is removed from the sample during the degassing process [13]. After this process the samples were heated to and maintained at the specific temperatures so that the thermionic emission intensity was either negligible, or comparable to the photo-induced emission intensity, and the photo-induced and thermionic emission spectra were then collected. Spectra obtained at elevated temperatures include contributions from photo-induced emission and thermionic emission. The thermionic emission data was subtracted from the combined spectrum in order to obtain the photo-induced emission component. This step has been previously described in more detail [5].

Photoelectron emission and thermionic emission electron microscopy (PEEM/ThEEM) measurements were performed with a prototype Elmitec LEEM III instrument. Samples were loaded onto a holder with integral heating and then inserted into the ultra-high vacuum microscope through a dry-pumped airlock. The sample temperature was controlled in a range from ambient to ~500 °C. During the heating experiments the pressure in the main chamber was maintained below 5×10^{-9} Torr. The voltage between the sample surface and anode was kept at a level of 10 kV, and the sample–anode distance was about 2 mm throughout the measurements. An Energetiq Laser Driven Light Source (LDLS), combined with selected optical band pass filters, was used for photo-excitation. The spectrum of the lamp is that of a xenon discharge source, with a nearly constant output from 170 nm to 800 nm. Due to field emission from high points on the sample, PEEM/ThEEM imaging of the N-doped diamond emitters was only possible from the samples on polished substrates [10]. The images were recorded with the UV "light-on" (total emission) and "light-off" (thermionic emission). To obtain an image of the photo-induced emission from a heated sample, the thermionic component was subtracted from the total emission using the image acquisition and processing program (Actos WinView).

3. Results

In order to compare the effects of different layers, optical absorbance measurements were taken from an efficient emitter diamond sample and one without the top N-diamond layer, both on similarly polished fused silica substrates. Data are shown in Fig. 1, which span from 200 to 900 nm. Comparison between the two curves suggests that a significant portion of the light was absorbed in the (N)UNCD layer, and the absorption was stronger in the UV regime. When the wavelength was below 300 nm, the optical absorbance increased significantly to the point that the signal intensity was below the detection limit of the instrument. Restricted by this detection limit, we suggest that this increase is possibly due to absorption from grain boundaries, defects, and diamond band gap transitions.

Fig. 2 shows the photoelectron spectra from sample D2 and D3 under He I (21.2 eV) photon illumination. Effective respective work functions of ~1.8 eV and 2.7 eV were deduced from the energy difference of the Fermi level (at 21.2 eV binding energy) and the back cut-off of the UPS spectrum. For semiconductors, the front and back cut-offs of a UPS scan follow the relationship:

$$\chi = E_V + \Phi_W - E_G, \tag{1}$$

where E_V is the front cut-off (the valence band maximum), Φ_W is the back cut-off (the work function), E_G is the bandgap of the material, and χ is the electron affinity (which is 0 for NEA materials). Because of the weak emission from the valence band maximum states, we have used this expression to determine the VBM assuming an NEA and then comparing the value with the extrapolation of the states

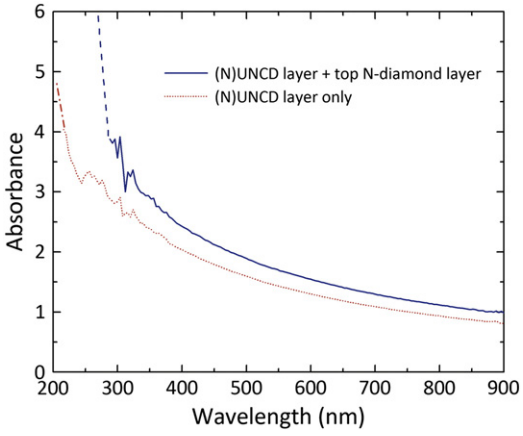

Fig. 1. Optical absorbance of the diamond structures, obtained through UV–vis spectroscopy measurements. The samples are diamond films deposited on polished transparent fused silica substrates, one with only the (N)UNCD layer and the other has a top N-diamond layer in addition. The dashed parts in the curves are extrapolated beyond the detection limit.

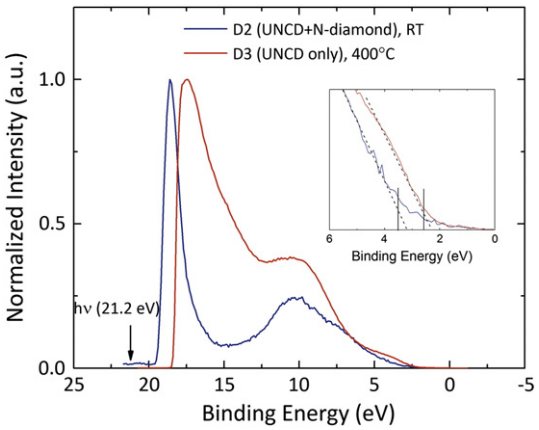

Fig. 2. UV photoemission spectra of samples D2 and D3. Linear fits of the valence band edges are shown as dashed lines in the inset, while the deduced values from a 5.4 eV bandgap were indicated by solid lines. The results indicate a negative electron affinity (NEA) for both samples.

near the VBM. The position of E_V is determined from Eq. (1) using the effective work function values noted above, the value of $\chi = 0$ for an NEA, and a bandgap of 5.4 eV for diamond films. Using this method the valence band edges were deduced at 3.6 eV and 2.7 eV below the Fermi level (indicated by the vertical bars in the Fig. 2 inset), and as indicated in the inset these values are similar to those obtained from fitting the experimental results [14]. Thus the UPS results are consistent with an NEA for the film surfaces.

The low energy electron emission spectra measured from the various samples are shown in Fig. 3 in the same sequence as listed in the sample preparation section. The spectra are shown for thermionic emission ("light-off") at an elevated temperature (denoted as "TE") and combined emission ("light-on") at different illumination wavelengths (denoted as "TE + PE" with the corresponding wavelength). The *x*-axis represents the kinetic energy of the emitted electrons relative to the Fermi level. As noted previously, assuming that thermionic and photo-induced emission are independent processes, the photo-induced electron spectra were obtained by subtracting the thermionic component from the combined emission data. Fig. 4 shows the thermionic and combined emission spectra and the resultant photo-induced emission components for 340 nm (3.65 eV) illumination.

The threshold energies for thermionic electron emission ("TE") and photo-induced electron emission ("PE") are of particular interest. The effective work function Φ_W for these NEA materials is defined as the energy difference between the conduction band edge of diamond and the Fermi level. A prior study has demonstrated that the low energy cut-off of the thermionic emission spectrum equals that of the UV photoemission spectrum at the diamond surface as measured by the same electron spectroscopy system, both of which represented Φ_W [15]. Here the data shows that, sample D1 exhibits the same low energy cut-off for both emission processes. When either the substrate or the interlayer was changed, larger thresholds for PE were observed. Comparing D2 with a bead-blasted Mo substrate to D1, sample D2 exhibited a PE threshold of ~2.2 eV. In Fig. 4(b), this value can be determined from the wavelength dependence of the photo-induced emission spectra. Here the two peaks indicate TE (at low kinetic energy) and PE (at higher kinetic energy). However, when only (N)UNCD was grown on the bead-blasted Mo substrate (sample D3), TE and PE again shared the same threshold, but at a higher energy of ~2.7 eV.

As shown in Figs. 3(d) and 4(d), a more complex spectrum was observed on sample D4 with the polished Mo/nanodiamond/N-diamond structure, which had a different interlayer compared to sample D1. Besides the effective work function of ~1.8 eV, which represents the thermionic emission threshold, a cut-off at approximately 2.4 eV and another near 3.0 eV are evident in the photo-induced emission spectra.

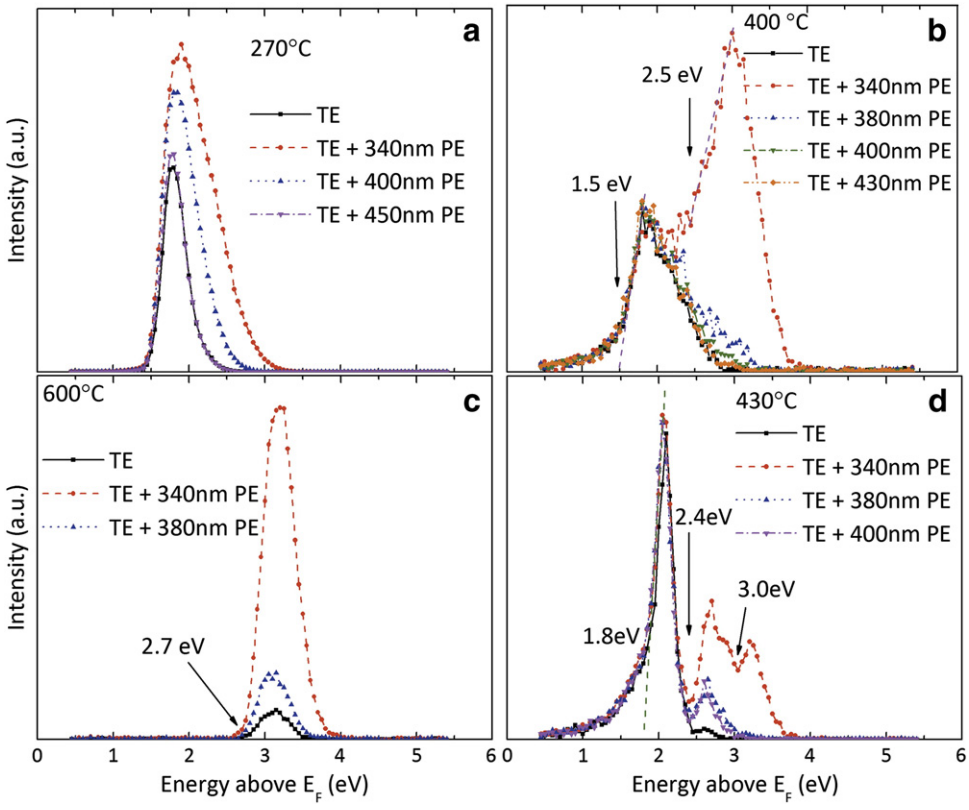

Fig. 3. Combined photo-induced and thermionic emission spectra from N-doped diamond films at elevated temperatures, showing the photon energy dependence. The results are shown following the sample sequence of (a) D1; (b) D2; (c) D3; and (d) D4.

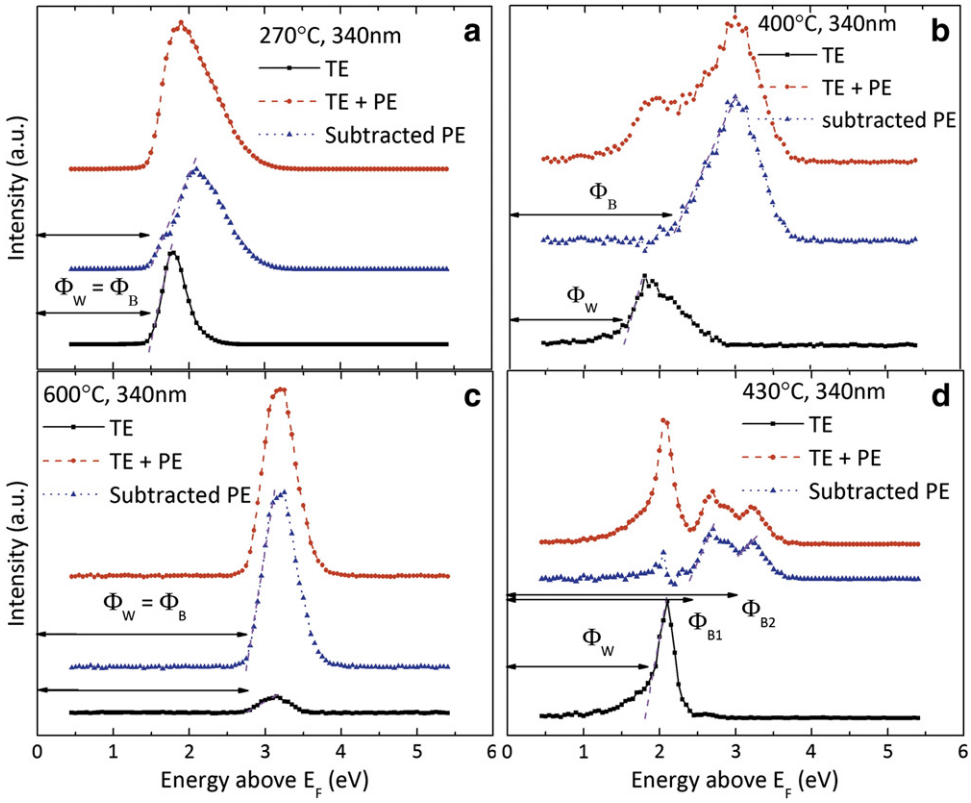

Fig. 4. The total emission, thermionic emission, and subtracted photo-induced emission spectral components from the diamond samples. Samples are listed in the same sequence as Fig. 2. Φ_B represents the threshold for photo-induced emission.

The cut-off at 3.0 eV may represent a separate barrier or a part of the electronic band structure above 2.4 eV. As the photo-induced emission component of the spectra shows significant wavelength dependence, this 3.0 eV structure was only observed when the excitation photons have an energy sufficiently high to support a detectable flux of electrons above this energy barrier (in this figure 340 nm light was used, equivalent to ~3.65 eV photons). Nevertheless, the photo-induced emission from all samples tested, excluding D1, appears to show an energy barrier between 2.2 and 2.7 eV, which could be a result of the same mechanism. It is possible that the same barrier also exists in D1 but is hidden due to the dominating electron emission over the lower threshold (the surface work function).

To further confirm these photo-induced emission thresholds, the PE components of D2 and D4 are shown in Fig. 5. The narrow peak near the TE cut-off in Fig. 5(b) is presumed to be a subtraction artifact caused by a peak shift between the two original spectra (Fig. 4(d)). Comparison between photo-induced emission spectra obtained at lower and higher temperatures is presented in the figure. At the lower temperature thermionic emission is negligible, while at the higher temperature the thermionic emission intensity is comparable with the photo-induced emission, and the TE is subtracted. The low energy cut-off appears to shift slightly to lower energy when temperature increases, which could be a result of increased scattering as electrons transit the diamond film [5]. While the results indicate that temperature may weakly affect the photo-induced emission intensity, the photo-induced emission thresholds were approximately constant.

PEEM/ThEEM images shown in Fig. 6 were obtained from sample D4 (polished Mo/nanodiamond/N-diamond). These images, which are similar to emission images from other samples of type D1 [10], display a relatively uniform spatial distribution of intensity from both TE and PE processes. Variations in the images are partially due to projection shadows from the 16° incident angle of the photons, and the polish scratches in the Mo substrate. The latter contributes to the parallel

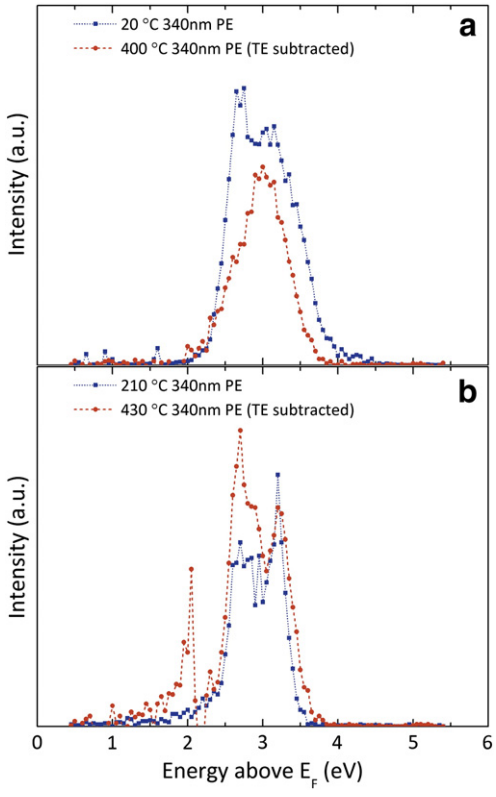

Fig. 5. Photo-induced emission spectra of samples (a) D2 and (b) D4 under illumination of the same wavelength, showing comparison between lower (no observable TE) and higher (significant TE observed) temperatures. In both cases the TE is subtracted from the 400 °C or 430 °C spectra.

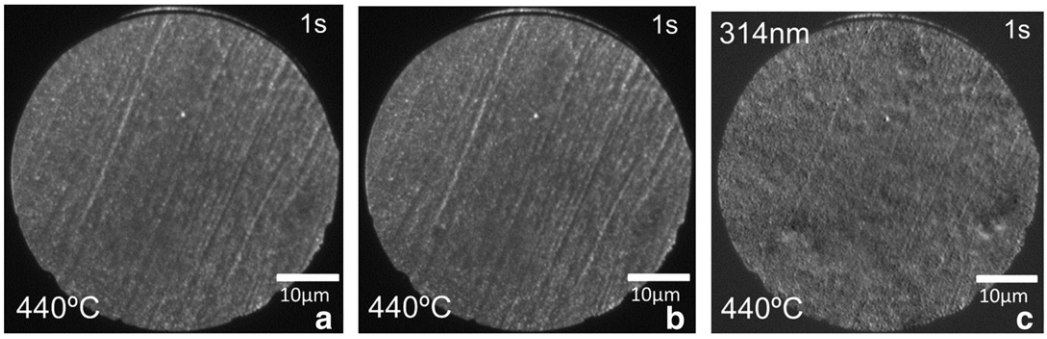

Fig. 6. PEEM images of (a) combined emission ("light-on"), (b) thermionic emission ("light-off") and (c) subtracted photo-induced emission from the sample with polished Mo substrate/nanodiamond/N-diamond structure (configuration D4).

line pattern in the images. The photon energy used for the PEEM image was 3.95 eV (314 nm).

4. Discussion

The spectroscopic results show several intriguing features of the low energy photo-induced emission. From all samples tested, the emitted electrons present a low energy cut-off that can be observed from the thermionic emission. Yet, unlike the thermionic emission spectra, the photo-induced emission spectra extend to a maximum kinetic energy that approximately corresponds to the respective photon energy. Assuming Spicer's three-step model for photoelectron emission [16], photo excited electrons are generated which transit to the sample surface and may be emitted into vacuum. The observed electron energy distribution indicates that the photo-excited electrons are generated at states near the Fermi level. Due to the wide band gap of diamond (~5.5 eV at ambient temperature), it was proposed that the sub-bandgap photons are transmitted through the diamond film and excite electrons at or near the metal–diamond interface [5].

The UV–vis results of the optical absorbance in the diamond films show that the (N)UNCD exhibits significant optical absorption. The results of photothermal deflection spectroscopy studies [17] also showed that the optical absorption of nitrogen-incorporated nanocrystalline diamond is not negligible. This suggests that photo-excited electrons will also be generated in the diamond film. Nitrogen doping and the consequent shift of E_F may lead to filling of the in-gap states, and the photoelectrons are likely generated from these populated states.

UV–vis reflectance data also showed that, optical absorption in the top N-diamond layer increases with photon energy, but is generally weaker than in the (N)UNCD layer. By comparing the emission spectra of the second and third sample configurations, it is shown that a higher thermionic emission threshold was observed without the top layer (Figs. 3(c) and 4(c)), and detecting the TE signal required higher temperatures. It appears that the main effect of the top N-doped diamond layer is to provide a low effective work function surface for the thermionic emission.

The difference observed in the electron emission spectra indicates that the interface and interlayer of the diamond emitters have a substantial effect on the emission characteristics. The origin of the observed energy barriers is not evident, and several possible mechanisms are discussed here. The first hypothesis would relate these thresholds to spatially separated regions on the surface. For instance, carbon patches were suggested to provide sub-bandgap photo-emission from B-doped single crystal diamond [18]. This suggestion leads to the need for microscopic studies on these samples. While the PEEM images show patches of lower intensity that may be due to surface roughness or variations in work function across the sample, the relatively uniform emission observed from the PEEM/ThEEM images suggests that either the spectral structures are not likely formed by separated domains, or the size of these domains is below the resolution limit for the PEEM images which is ~125 nm for these images. An alternative hypothesis is that the additional spectral features result from variations in the electronic structure. Different local bonding configurations of the substrate and interlayer may lead to changes in the band structure and density of states. This includes several possibilities:

A. Changes of the initial states in the photo-generation process could alter the distribution of available electrons from the ideal metal parabolic band model.
B. The transport of electrons through the (N)UNCD layer may depend on specific states in the complex nanocrystalline material.
C. The diamond/metal interface may produce a Schottky barrier higher than the surface work function and provide a second barrier.

It is likely that the observed photo-induced emission characteristics are due to a combination of these effects. Nevertheless, it appears that the (N)UNCD layer can significantly contribute to this process. The electronic states of the sp^2 bonds abundant in this layer [19,20] may result in distinct conductive states corresponding to the additional generation and transmission paths, and possibly affect the interface barriers. As sp^2 bonds in nanocrystalline diamond exist mostly at the grain boundaries, spatial measurements of this process are below the spatial resolution of PEEM due to the small grain size (<10 nm), and may require other techniques in further research. While the results here also indicate the possible effects of substrate morphology on the photo-induced emission process, the mechanism relating it to the electronic structure of the samples is beyond the scope of this work.

This model proposes that the photo-induced electrons are transported through the diamond film. An important question is how electron scattering and recombination affect the observed spectra. The process involves two effects: recombination that limits the diffusion length and thermalization (electron scattering) that would change the energy distribution. Prior studies have shown electron diffusion lengths from ~5 to greater than 100 μm for polycrystalline and single crystal diamond [21–24]. While the actual diffusion length in the UNCD layer may be lower, diffusion of electrons from the substrate through the diamond is anticipated to be efficient. Our previous study of a sample like D1 showed a high energy tail that correlated to the photon energy. The spectral shape was described by the "thermalization" of the electrons through phonon scattering. The numerical simulation including optical phonon scattering described the experimental spectra with a fit value of ~8–9 optical phonon scattering events in transitioning to the surface [5]. We note that diamond is non-polar and the electron–phonon scattering processes are less efficient than for polar semiconductors. Hence the electrons generated at the diamond/metal interface may be able to transport to the diamond surface and at least partially reflect the photo-generated electron energy distribution. However, these considerations may not be sufficient to describe the different emission thresholds observed for some samples, which may indicate a more complex transport process.

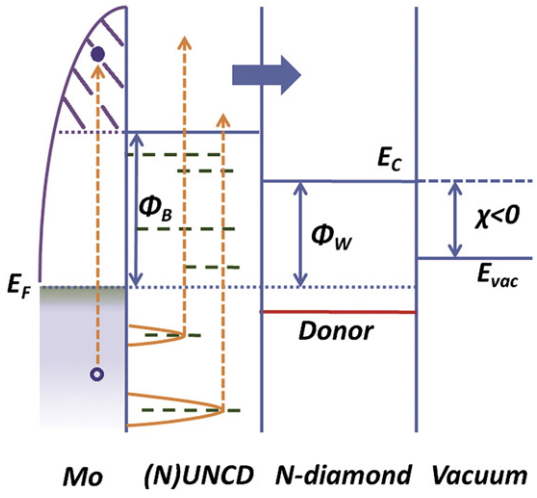

Fig. 7. Band schematics of the diamond emitter. Photo-electrons are presumed to be generated in the UNCD layer or near the metal–diamond interface. Dashed lines represent inter-bandgap states introduced by sp^2 bonds.

The emission mechanisms involving these effects are shown in the band diagram of Fig. 7. In this model, the observed photo-induced electron emission involves photo-excited electrons from both the diamond–metal interface and the populated states in the (N)UNCD layer. The electrons transport through the conduction channels in the film and are emitted from the surface layer into vacuum. The photo-induced emission threshold may be increased if an extra energy barrier is present, which may arise from the initial state distribution, the presence of conduction channels, or other interface effects.

5. Conclusion

Combined photo-induced and thermionic electron emission of nitrogen-doped, hydrogen-terminated diamond samples was examined with different interface and interlayer conditions between the metal substrate and the top N-doped diamond film. Multiple photo-induced emission thresholds were observed with sub-bandgap photons. PEEM imaging shows that these thresholds were either due to variation of the electronic structure of the different sample sets, or from separated emissive domains, the size of which was below the image resolution. This indicates the effects of the interface and interlayer on the photo-induced electron generation, transition and emission. The relationship between interface bonding and morphology and the electronic structure of the film is yet uncertain. While the underlying physics requires further exploration, the results discussed above indicate its importance in affecting the emission characteristics. Thus, the phenomena reported in this study call for detailed studies to optimize the design of diamond based photo-induced electron emitters.

Prime novelty statement

Hydrogen terminated and nitrogen-doped diamond films exhibit a low work function. This research investigated photo-induced and thermionic electron emission from a range of nitrogen-doped diamond films deposited on molybdenum substrates. The results show that the interface properties of the films can substantially affect the characteristics of the electron emission spectrum.

Acknowledgments

This research was supported through the Office of Naval Research under contract number N00014-10-1-0540. The authors thank Gary G. Hembree for technical support for PEEM imaging. We gratefully acknowledge the LeRoy Eyring Center for Solid State Science at Arizona State University and Diana Convey for the use of the UV–vis spectrometer.

References

[1] F.J. Himpsel, J.A. Knapp, J.A. VanVechten, D.E. Eastman, Quantum Photoyield of Diamond (111) - A Stable Negative-Affinity Emitter, Phys. Rev. B 20 (1979) 624.
[2] B.B. Pate, The Diamond Surface: Atomic and Electronic Structure, Surf. Sci. 165 (1986) 83.
[3] J. van der Weide, Z. Zhang, P.K. Baumann, M.G. Wensell, J. Bernholc, R.J. Nemanich, Negative-Electron-Affinity Effects on Diamond (100) Surface, Phys. Rev. B 50 (1994) 5803.
[4] F.A.M. Koeck, R.J. Nemanich, Low Temperature Onset for Thermionic Emitters Based on Nitrogen Incorporated UNCD Films, Diam. Relat. Mater. 18 (2009) 232–234.
[5] T. Sun, F.A.M. Koeck, C. Zhu, R.J. Nemanich, Combined Visible Light Photo-Emission and Low Temperature Thermionic Emission from Nitrogen Doped Diamond Films, Appl. Phys. Lett. 99 (2011) 202101.
[6] K. Uppireddi, T.L. Westover, T.S. Fisher, B.R. Weiner, G. Morell, Thermionic Emission Energy Distribution from Nanocrystalline Diamond Films for Direct Thermal-Electrical Energy Conversion Applications, J. Appl. Phys. 106 (2009) 043716.
[7] F.A.M. Koeck, R.J. Nemanich, Emission Characterization from Nitrogen-Doped Diamond with Respect to Energy Conversion, Diam. Relat. Mater. 15 (2006) 217–220.
[8] J.D. Rameau, J. Smedley, E.M. Muller, T.E. Kidd, P.D. Johnson, Properties of hydrogen terminated diamond as a photocathode, Phys. Rev. Lett. 106 (2011) 137602.
[9] J.W. Schwede, I. Bargatin, D.C. Riley, B.E. Hardin, S.J. Rosenthal, Y. Sun, F. Schmitt, P. Pianetta, R.T. Howe, Z.X. Shen, N.A. Melosh, Photon-enhanced thermionic emission for solar concentrator systems, Nat. Mater. 9 (2010) 762–767.
[10] N. Neugebohrn, T. Sun, F.A.M. Koeck, G.G. Hembree, R.J. Nemanich, T. Schmidt, J. Falta, Spatial Correlation of Photo-Induced and Thermionic Electron Emission from Low Work Function Diamond Films, Diam. Relat. Mater. 40 (2013) 12–16.
[11] F.A.M. Koeck, R.J. Nemanich, Y. Balasubramaniam, K. Haenen, J. Sharp, Enhanced Thermionic Energy Conversion and Thermionic Emission from Doped Diamond Films Through Methane Exposure, Diam. Relat. Mater. 20 (2011) 1229–1233.
[12] O.A. Williams, Nanocrystalline Diamond, Diam. Relat. Mater. 20 (2011) 621–640.
[13] T. Haensel, J. Uhlig, R.J. Koch, S.I.U. Ahmed, J.A. Garrido, D. Steinmüller-Nethl, M. Stutzmann, J.A. Schaefer, Influence of Hydrogen on Nanocrystalline Diamond Surfaces Investigated with HREELS and XPS, Phys. Status Solidi A 206 (2009) 2022–2027.
[14] J. van der Weide, R.J. Nemanich, Schottky Barrier Height and Negative Electron Affinity of Titanium on (111) Diamond, J. Vac. Sci. Technol. B 10 (1992) 1940.
[15] M. Kataoka, C. Zhu, F.A.M. Koeck, R.J. Nemanich, Thermionic Electron Emission from Nitrogen-Doped Homoepitaxial Diamond, Diam. Relat. Mater. 19 (2010) 110–113.
[16] W.E. Spicer, Photoemissive, Photoconductive, and Optical Absorption Studies of Alkali-Antimony Compounds, Phys. Rev. 112 (1958) 114.
[17] P. Achatz, J.A. Garrido, M. Stutzmann, O.A. Williams, D.M. Gruen, A. Kromka, D. Steinmüller, Optical Properties of Nanocrystalline Diamond Thin Films, Appl. Phys. Lett. 88 (2006) 101908.
[18] J.B. Cui, J. Ristein, L. Ley, Low-Threshold Electron Emission from Diamond, Phys. Rev. B 60 (1999) 16135.
[19] S. Bhattacharyya, Mechanism of High N-Type Conduction in Nitrogen-Doped Nanocrystalline Diamond, Phys. Rev. B 70 (2004) 125412.
[20] K. Subramanian, W.P. Kang, J.L. Davidson, R.S. Takalkar, B.K. Choi, M. Howell, D.V. Kerns, Enhanced Electron Field Emission from Micropatterned Pyramidal Diamond Tips Incorporating CH4/H2/N2 Plasma-Deposited Nanodiamond, Diam. Relat. Mater. 15 (2006) 1126–1131.
[21] J. Ristein, W. Stein, L. Ley, Defect Spectroscopy and Determination of the Electron Diffusion Length in Single Crystal Diamond by Total Photoelectron Yield spectroscopy, Phys. Rev. Lett. 78 (1997) 1803–1806.
[22] V. Richter, B. Fizgeer, Sh. Michaelson, A. Hoffman, R. Kalish, Escape Depth of Secondary Electrons Induced by Ion Irradiation of Submicron Diamond Membranes, 96 (2004) 5824.
[23] T. Teraji, S. Yoshizaki, S. Mitani, T. Watanabe, T. Ito, Transport Properties of Electron-Beam and Photo Excited Carriers in High-Quality Single-Crystalline Chemical-Vapor-Deposition Diamond Films, J. Appl. Phys. 96 (2004) 7300.
[24] J.E. Yater, A. Shih, R. Abrams, Electronic Properties of Diamond for High-Power Device Applications, Solid State Electron. 42 (1998) 2225–2232.